Supplemental Material

Supplemental Methods

Eligibility criteria: Full entry and exclusion criteria appear in Table S1.

Proprioception Assessment: Prior to testing each hand, subjects performed passive range of motion exercises using the FINGER robot to ensure no pain or discomfort. The examiner then walked through a practice round with each subject, confirming that they understood and could demonstrate the task. Next, appropriate attention and cognitive status were confirmed, with the method being that each subject was required to correctly repeat full task instructions to the examiner. During practice, to teach participants how to perform the task, subjects were permitted to see their fingers, but during the trials when study data were collected, their view of their fingers was obscured by a cloth placed over the robot and their hand. They also wore noise-canceling headphones to block out the sound of the robot. The robot-guided finger-crossing movements during the task were relatively slow, and as a result identification of direct finger alignment was not dependent on reaction time, as subjects were able to anticipate the moment of finger crossing. This was demonstrated in our previous study of unimpaired control subjects, wherein about half of the proprioception errors were made before and half following direct finger alignment[1]. Thus, this proprioception task with the FINGER robot measures ability to integrate proprioceptive information during relatively slow movement of the fingers to detect direct finger alignment.

Proprioception error as reported here reflects the average of the absolute error across the 12 finger-crossing movements for each hand of each subject.

The robot was controlled by a PC running the Mathworks XPC Target real-time operating system with a control loop running at 1000Hz. The crossing experiment was implemented by a

second computer (the XPC host) that communicated with the XPC target PC over a wired TCP connection. In addition to sending commands to the robot and receiving sensor updates, the XPC host computer also listened for keyboard events. Since both of these actions were performed by the same machine, no additional synchronization was necessary. Standard keyboards, such as the one used here, have a latency of 20 - 40 ms. Given that the fingers moved at a maximum speed of 13 degrees/sec, a 40-msec keyboard latency would thus contribute an error of up to 0.5 degree for each finger, i.e., 1 degree of total separation error.

Thalamocortical sensory tract (TST) injury: The normal TST was developed with diffusion tensor imaging (DTI) from 17 healthy control subjects[2] (Fig. 1). In native space, images were first corrected for eddy current distortions and head motion artifacts using FSL (www.fmrib.ox.ac.uk/fsl). FSL's BEDPOSTX program was then used to generate probability distributions of diffusion parameters at each voxel, including modeling for diffusion of crossing fibers along two directions. With the thalamus as the seed region, connectivity-based segmentation was used to assign each voxel in the seed some probability of being connected to each of various targets, including the post-central gyrus. Subject-specific masks of thalamic regions with highest probability of connection to the post-central gyrus were generated. Each mask was visually inspected and compared to an anatomical atlas[3], confirming that they were located in the approximate region classically defined as the ventral posterolateral (VPL) nucleus. Next, probabilistic tractography was performed in each subject using the dorsal two-thirds of the post-central gyrus as the seed region, the VPL nucleus as a waypoint target mask, and a mid-sagittal slice as an exclusion mask. The resulting individual subject tracts were binarized, transformed into MNI space, summed, and thresholded to include only voxels that were common to the tracts of ≥6 subjects. Similar to methodology we have used to calculate percent injury to

the CST[1-6], percent injury to the TST was calculated by dividing the tract into 16 vertical strings and expressing percent injury as the percent of these 16 vertical strings that has at least 5% overlap between a given infarct and the normal TST. This approach aims to use vertical strings to model the trajectory of groups of axons. The goal is to classify each vertical string as injured or not--a string only needed to be damaged by stroke once along its length for it to be classified as injured. This approach contrasts with methods that calculate injury to a tract by measuring total overlap between infarct and tract, whereby injury to an axon at multiple points along its length is counted as an increased extent of injury. Because of seed point locations, values for white matter injury for subjects with infarcts inferior to the thalamus were omitted from statistical analyses.

Functional activation: Functional data from the four BOLD fMRI runs were preprocessed using the Statistical Parametric Mapping 12 (SPM12) software (http://www.fil.ion.ucl.ac.uk/spm/). Preprocessing steps included realignment to the first image, coregistration to the mean EPI image, normalization to the standard MNI EPI template, and spatial smoothing (FWHM = 6 mm). Data were visually inspected for head movement and were rejected for subjects with >2mm head displacement.

For statistical analysis, the fMRI data were modeled as a boxcar convolved with a hemodynamic response. A high-pass filter of 128 seconds was used to remove low signal changes. Functional run data were inspected for outliers due to excessive head motion (>1 mm translation or >0.2 radians rotation between each volume) and signal noise (Z>3 from the mean image intensity) using the Artifact Detection Tool (http://www.nitrc.org/projects/artifact_detect). Outliers were de-weighted during statistical analysis. Single-subject t-maps (task versus rest) were generated using a threshold of $p < 0.001$ uncorrected for multiple comparisons. Activation

volume and contrast estimates were then extracted in SPM12 using small volume correction for M1, S1, and S2 ROIs on each brain side.

Functional connectivity: Movement emerges from the interactions between different brain regions within a distributed network. Studies that measure functional activation in an isolated brain region do not completely explain how spatially separated brain regions interact in support of motor behavior. Functional connectivity methods address this by measuring the temporal correlation between spatially remote neurophysiological processes, captured via their fMRI time courses. Functional connectivity between brain regions is thus measured based on the extent to which their fMRI time courses are correlated[7,8].

To measure functional connectivity, time courses from the fMRI data (above) were then filtered between 0.008 and 0.13 to minimize low-frequency drift and high-frequency noise. Within-subject realignment parameters, outliers, and main session effects were included as first-level covariates. Functional connectivity was then evaluated between ipsilesional M1 and contralesional M1, ipsilesional S1, and ipsilesional S2 (iM1-cM1, iM1-iS1, and iM1-iS2, respectively); between ipsilesional S1 and contralesional S1, and ipsilesional S2 (iS1-cS1, iS1-iS2, respectively); and between ipsilesional S2 and contralesional S2 (iS2-cS2). Primary analysis of S2 examined OP 4, as above, but OP 1[7] was also examined to enable secondary hypothesis testing. Fisher-transformed correlation coefficients were extracted for each connection in each subject.

Choice of ROIs: Spherical ROIs (6 mm radius) were used to probe the hand region of M1, the hand region of S1, and the OP 4 subregion of S2 bilaterally. A spherical ROI was employed because of its small and focal nature. Many atlases have ROIs that pertain to motor or sensory cortices, but typically these are very large ROIs that are not focused on the hand area, as was the

focus here. Spherical ROIs suffer from inclusion of both gray matter and white matter voxels, but this is also true for many atlas-based ROIs.

Threshold for abnormal proprioception error: Figure 3 classifies patients as having normal or abnormal proprioception error using a discrete threshold of >2SD beyond normative values from a cohort of age-matched, neurologically intact, healthy control subjects. A secondary approach to understanding errors in patients' relative to healthy control subjects' errors, one that is independent from arbitrary thresholding, was also performed. Logistic regression was performed, using proprioception error (for patients, in the contralesional hand; for healthy control subjects, the average of dominant and non-dominant hands) as the independent variable and disease status (stroke vs. control) as the dependent variable. This generated a receiver operating characteristic (ROC) curve from which area under the curve (AUC) was calculated.

Table S1. Inclusion and Exclusion Criteria

Entry Criteria

1. Age ≥18 and ≤ 80 years
2. Stroke onset >6 months prior
3. Residual hand motor deficit was present (B&B score in the stroke-affected hand must be ≤90% of the score in the non-affected hand)
4. Preserved voluntary hand movements was also present (B&B score in the stroke-affected hand must be ≥3 blocks over 60 sec)

Exclusion Criteria

1. Contraindication to MRI
2. Severe cognitive impairment
3. Concurrent diagnosis affecting arm/hand function
4. Hand motor status not at stable plateau (change in B&B score >6 between the two baseline visits)

Supplemental Results

Proprioception error and motor status: Given that proprioception testing of one hand required metacarpophalangeal joint flexion of the opposite hand to press the spacebar, it is important to assess the relationship between proprioception error of the tested hand and motor status of the opposite hand. There was a weak relationship between contralesional hand proprioception error and ipsilesional FT score ($r=-0.43$, $p=0.03$). However, this correlation explained only 18% of variance in contralesional proprioception error and was not significant when accounting for age, a covariate previously demonstrated to be of importance when assessing proprioception using FINGER in a healthy population[1]. Moreover, the trial-to-trial variance in proprioception testing had no relationship with finger motor status of ipsilesional hand ($p=0.8$). Proprioception error in the ipsilesional hand was not related to motor status (FT score) of the contralesional hand.

ROC Curve: The ability for proprioception error to distinguish patients with stroke from healthy control subjects was examined using an ROC curve (Supplemental Figure 1). Performance was good, with area under the curve (AUC) of 0.883.

Supplemental Discussion

Prediction of finger crossing might be based on finger position sense or finger movement sense. We believe that the current approach measured finger position sense because if finger movement sense were the main contributor, the motor system would have to integrate the sense of movement of both fingers to predict the exact position at which the fingers cross, which seems unlikely. On the other hand, there is a difference between sensing absolute finger position (i.e., finger position relative to an absolute position in space) and relative finger position (i.e., finger position relative to another finger). The motor system is better at detecting relative finger position than absolute position[9]. The approach employed in the current study tested relative finger position sense.

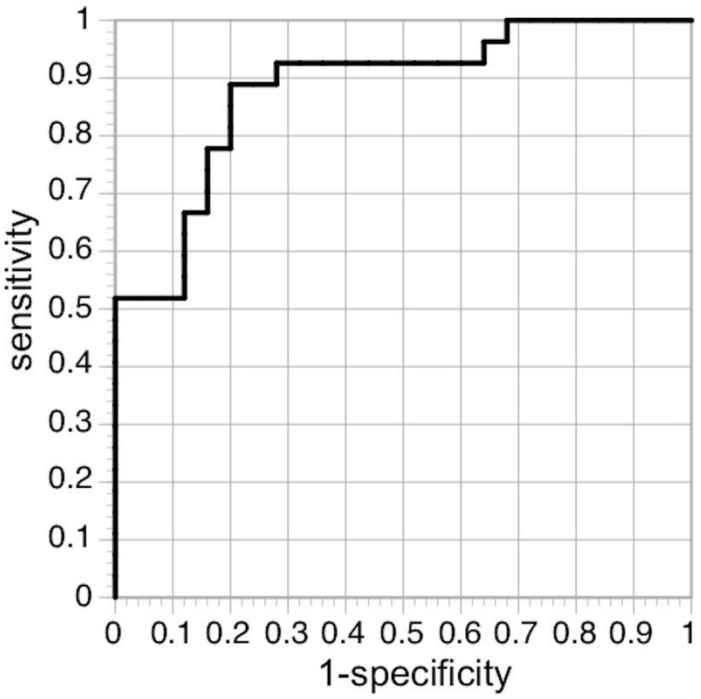

Supplemental Figure 1. The ability for proprioception error to distinguish patients with stroke from healthy control subjects was examined using an ROC curve, which displays sensitivity (true positive rate) as a function of 1-specificity (false positive rate). This curve showed an AUC = 0.883.

Supplemental References

1. Riley JD, Le V, Der-Yeghiaian L, et al. Anatomy of stroke injury predicts gains from therapy. *Stroke.* 2011;42(2):421-426.
2. Nouri S, Cramer SC. Anatomy and physiology predict response to motor cortex stimulation after stroke. *Neurology.* 2011.
3. Dodakian L, Sharp KG, See J, et al. Targeted engagement of a dorsal premotor circuit in the treatment of post-stroke paresis. *NeuroRehabilitation.* 2013;33(1):13-24.
4. Burke Quinlan E, Dodakian L, See J, et al. Neural function, injury, and stroke subtype predict treatment gains after stroke. *Ann Neurol.* 2015;77(1):132-145.
5. Wu J, Quinlan EB, Dodakian L, et al. Connectivity measures are robust biomarkers of cortical function and plasticity after stroke. *Brain.* 2015;138(Pt 8):2359-2369.
6. Cassidy JM, Tran G, Quinlan EB, Cramer SC. Neuroimaging identifies patients most likely to respond to a restorative stroke therapy. *Stroke.* 2018;49(2):433-438.
7. Grefkes C, Fink GR. Reorganization of cerebral networks after stroke: new insights from neuroimaging with connectivity approaches. *Brain.* 2011.
8. Varsou O, Macleod MJ, Schwarzbauer C. Functional connectivity magnetic resonance imaging in stroke: an evidence-based clinical review. *Int J Stroke.* 2014;9(2):191-198.
9. Dandu B, Kuling I, Visell Y. Proprioceptive Localization of the Fingers: Coarse, Biased, and Context-Sensitive. *IEEE Trans Haptics.* 2019.